Self-assembly of long chain alkanes and their derivatives on graphite

Teng Yang,[1] Savas Berber,[1] Jun-Fu Liu,[2] Glen P. Miller,[2] and David Tománek[1,a)]
[1]*Physics and Astronomy Department, Michigan State University, East Lansing, Michigan 48824-2320, USA*
[2]*Department of Chemistry and Materials Science Program, University of New Hampshire, Durham, New Hampshire 03824, USA*

(Received 5 November 2007; accepted 16 January 2008; published online 28 March 2008)

We combine scanning tunneling microscopy (STM) measurements with *ab initio* calculations to study the self-assembly of long chain alkanes and related alcohol and carboxylic acid molecules on graphite. For each system, we identify the optimum adsorption geometry and explain the energetic origin of the domain formation observed in the STM images. Our results for the hierarchy of adsorbate-adsorbate and adsorbate-substrate interactions provide a quantitative basis to understand the ordering of long chain alkanes in self-assembled monolayers and ways to modify it using alcohol and acid functional groups. © *2008 American Institute of Physics*. [DOI: 10.1063/1.2841478]

I. INTRODUCTION

The controlled self-assembly of molecules to form ordered nanoscale patterns is an area of active research. These superstructures often exhibit unusual properties[1] and are finding numerous applications in nanotechnology, including use as nanotemplates.[2] Nanotemplates enable directed assembly of nanoscale objects and allow for the transfer of those patterned objects to receiving substrates. For example, as nanoparticles can be selectively attached to either molecular or polymeric species, nanotemplates derived from self-assembled molecules or polymers provide an efficient means to prepare ordered arrays of uniformly spaced nanoparticles. Nanotemplates of this type permit feature sizes and feature densities that are unrivaled by current lithographic techniques including electron-beam nanolithography and scanning probe methods such as dip-pen nanolithography[3] and field-assisted nanolithography.[4]

Self-assembled monolayers (SAMs) of molecular and polymeric species on highly oriented pyrolytic graphite (HOPG) have attracted much attention, since the formation of various adsorption patterns can be monitored using scanning tunneling microscopy (STM) methods.[5–8] Although many patterns have been reported even for alkane films on graphite, the energetic grounds for the optimum SAM structure have never been investigated. Since the interplay between adsorbate-adsorbate and adsorbate-substrate interactions ultimately determines the equilibrium geometry of the molecular assemblies, it should be possible to induce specific changes in the SAM superstructures by modifying the terminal functional groups of the molecules in a predetermined manner. Unfortunately, published STM data of SAMs on graphite do not provide a quantitative interpretation of the resulting superstructures and, therefore, do not allow for predictions concerning the effect of specific functional groups on the corresponding self-assembled superstructure.

Here, we study the self-assembly of long chain alkanes and their derivatives on graphite using a combination of STM measurements with *ab initio* electronic structure and total energy calculations. We identify the optimum adsorption geometry of the molecules and explain the energetic origin of the domain morphology observed by STM. Our electronic structure calculations allow a quantitative interpretation of the STM images. Calculated total energy results provide a quantitative basis for judging the ordering tendency of alkane chains in self-assembled monolayers and ways to modify the ordering using alcohol (OH) and carboxylic acid (COOH) functional groups.

II. COMPUTATIONAL DETAILS

To obtain fundamental insight into the origin of different adsorption patterns of long chain alkanes and their derivatives on graphite, we determined the equilibrium geometry, binding energy, and electronic structure of these systems under different conditions. Our calculations are based on the *ab initio* density functional theory (DFT) within the local density approximation (LDA).[9] We used the Perdew–Zunger[10] parametrized exchange-correlation functional, as implemented in the SIESTA code,[11] and a double-ζ polarized basis localized at the atomic sites. We used the counterpoise method[12] to avoid basis-set superposition errors introduced by the localized basis. The valence electrons were described by norm-conserving Troullier–Martins pseudopotentials[13] in the Kleinman–Bylander factorized form.[14] This computational approach is known to correctly describe the equilibrium geometries and energies associated with the alkane-alkane and alkane-HOPG interactions, as well as the strength of alcohol-alcohol and acid-acid hydrogen bonds.

Since adsorption of alkane chains on graphite and graphene should be very similar, we performed our calculations on infinite graphene monolayers using periodic boundary conditions. In the superlattice geometry modeling isolated monolayers, graphene layers were separated by 20 Å in the normal direction and represented by orthorhombic unit cells containing four carbon atoms. The supercells were

a)Electronic mail: tomanek@msu.edu.

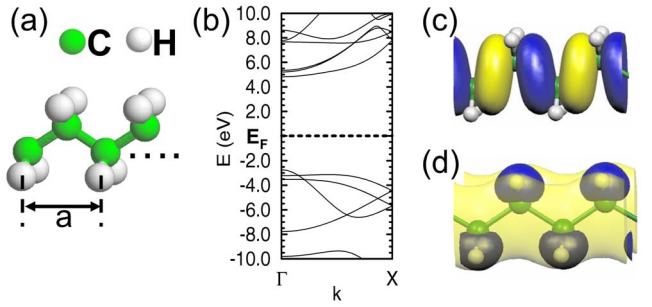

FIG. 1. (Color online) (a) Equilibrium geometry and (b) electronic band structure of an infinitely long polyethylene chain. Wave functions of the states at $k=\Gamma$ corresponding to (c) the top of the valence band and (d) the bottom of the conduction band are shown in the same perspective as used in (a). The wave function contours are presented for the amplitude $|\psi|=0.04a_0^{-3/2}$ and superposed with the atomic positions. The wave function phase is distinguished by color.

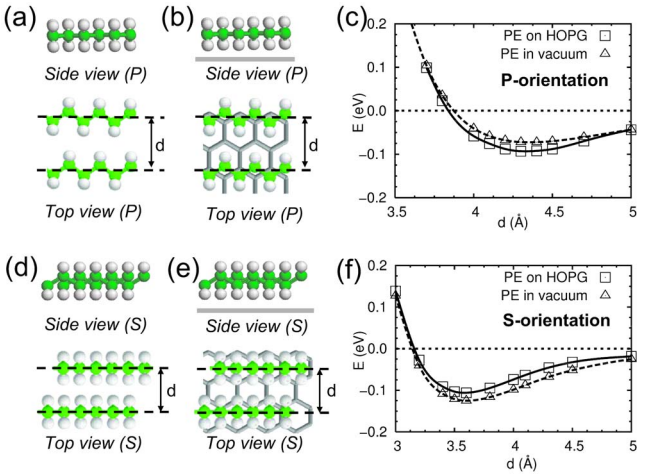

FIG. 2. (Color online) Interactions between two infinitely long polyethylene chains in [(a)–(c)] coplanar (*P*) and [(d)–(f)] stacked (*S*) arrangements. Interaction energies are plotted in (c) and (f) as a function of the interchain distance *d* for polymers in vacuum, depicted in (a) and (d), and polymers adsorbed on graphene, depicted in (b) and (e). Energy values per primitive unit cell of the polyethylene chain pair in vacuum are indicated by empty triangles and those for chains chemisorbed on graphene by empty squares in (c) and (f).

sampled by a $32\times32\times1$ *k*-point mesh. When modeling finite alkane chains on graphene, we used 3×5 graphene supercells with 60 C atoms and sampled the Brillouin zone by a $11\times7\times1$ *k*-point mesh. The self-consistent charge density was obtained using a real-space grid with a mesh cutoff energy of 250 Ry, sufficient to achieve a total energy convergence of better than 0.05 meV/atom during the self-consistency iterations.

III. EXPERIMENTAL

As a counterpart to the theoretical results, we observed overlayers of alkanes and their derivatives on graphite using STM. Saturated solutions of *n*-docosane (99%, Aldrich, Milwaukee, WI), 1-docosanol (97%, Aldrich, Milwaukee, WI), and 1-docosanoic acid (99%, Aldrich, Milwaukee, WI) were prepared in 1-phenyloctane (99.9%, Aldrich, Milwaukee, WI). A small drop of the solutions was spread onto a freshly cleaved surface of HOPG (ZYA grade, MikcroMasch, Wilsonville, OR). Scanning tunneling microscope imaging was performed under ambient conditions (21–23 °C) using a Nanoscope IIIa STM (Digital Instruments, Santa Barbara, CA) with platinum/iridium tips (Digital Instruments, Santa Barbara, CA). The STM was calibrated using freshly cleaved HOPG. Images were captured *in situ* in constant current mode at the HOPG-liquid interface, while integral and proportional gains were in the range of 2–5. The raw images were filtered to remove high frequency noise.

IV. RESULTS

A. Freestanding long chain alkanes

The equilibrium geometry and electronic structure of freestanding polyethylene, representing an alkane chain, is shown in Figs. 1(a) and 1(b). To represent isolated polymers in a superlattice geometry, we arranged them on a tetragonal lattice with a large interchain separation of 20 Å and sampled the rather short Brillouin zone of these one-dimensional structures by 16 *k* points. The optimized structure of freestanding polyethylene, with the carbon backbone forming a zigzag chain, is shown in Fig. 1(a). The primitive unit cell of length $a=2.55$ Å contains two C and four H atoms. The LDA band structure of the infinite chain, depicted in Fig. 1(b), suggests that polyethylene is a wide-gap insulator. The wave functions associated with the top of the valence band at Γ are shown in Fig. 1(c), those of the conduction band bottom at Γ are shown in Fig. 1(d). The spatial distribution of these frontier orbitals is useful for judging the nature of polymer-polymer and polymer-graphene interactions.

B. Structure and stability of long chain alkane monolayers

For long chain alkanes on graphite, controversy exists concerning whether the carbon skeletal plane should lie parallel,[15] perpendicular,[8] or at an ≈30° angle[16] to the graphite basal plane in the SAM superstructure. To help solve this controversy, we compared the total energies of the different structures and show our results in Fig. 2. We distinguish the *coplanar orientation* (*P*), where the zigzag carbon backbones of the alkanes or polyethylene, separated by the distance *d*, all lie in the same plane, from the *stacked orientation* (*S*), where all alkane or polyethylene chains are axially rotated by 90° and the zigzag carbon backbone planes are separated by *d* in the normal direction. On graphene, the *P* orientation of polyethylene in vacuum, depicted in Fig. 2(a), translates to that of polyethylene chains lying down parallel to graphene, as shown in Fig. 2(b). The energetic comparison in Fig. 2(c) suggests that the graphene substrate plays only a minor role in the interchain interaction. In particular, the equilibrium interchain distance of 4.26 Å in the coplanar orientation is nearly the same in vacuum and on graphene.

Similarly, the *S* orientation of polyethylene in vacuum, depicted in Fig. 2(d), translates to that of polyethylene chains adsorbed with their zigzag planes normal to the graphene substrate, as indicated in Fig. 2(e). Again, the equilibrium interchain distance of 3.50 Å in this geometry is very similar

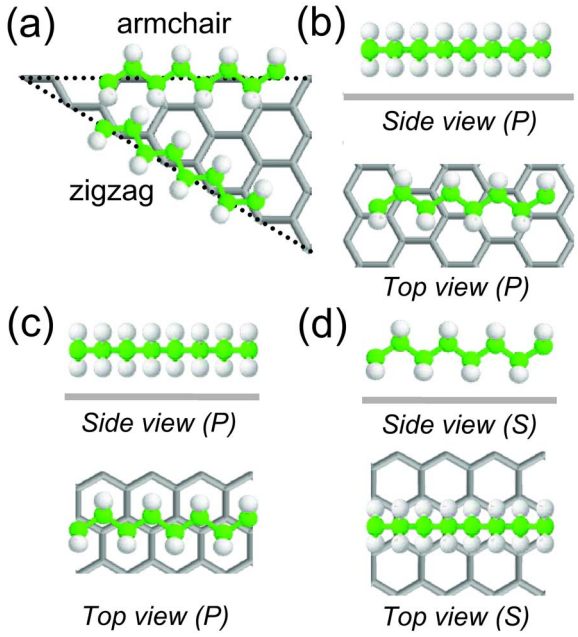

FIG. 3. (Color online) Alignment of polyethylene (PE) chains in different orientations on graphene. Polyethylene may lie parallel to graphene in the *P* orientation or normal to graphene in the *S* orientation. (a) Definition of armchair and zigzag directions on graphene. (b) PE(*P*) along the armchair direction, (c) PE(*P*) along the zigzag direction, and (d) PE(*S*) along the zigzag direction, viewed from the side or the top.

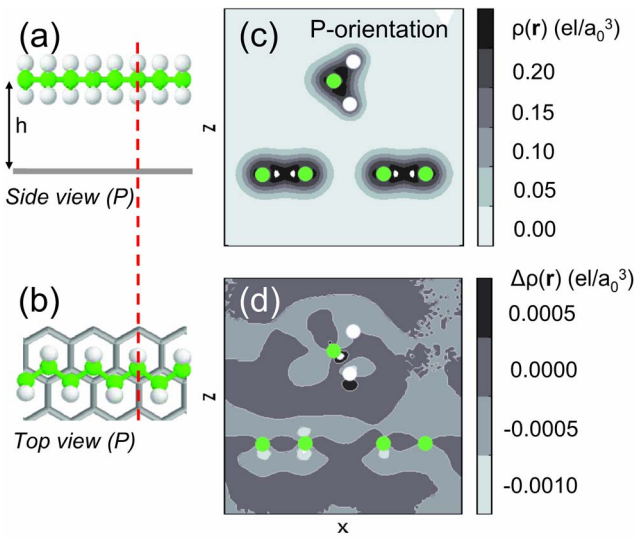

FIG. 4. (Color online) Nature of bonding of polyethylene in *P* orientation, lying parallel to graphene. The polyethylene adsorption geometry on graphene, shown (a) in side view and (b) in top view. Contour plots of (c) the total charge density $\rho_{PE/gra}(\mathbf{r})$ and (d) the charge density difference, defined as $\Delta\rho(\mathbf{r})=\rho_{PE/gra}(\mathbf{r})-\rho_{PE}(\mathbf{r})-\rho_{gra}(\mathbf{r})$. The plane of the contour plots is normal to the polymer axis and is indicated by the dashed line in (a) and (b).

on graphene and in vacuum, as seen in Fig. 2(f). Comparing energy values in Figs. 2(c) and 2(f), we find that the interchain attraction leads to an energy gain of $\approx$0.1 eV/C_2H_4 with respect to separated polymers, both in the coplanar (*P*) and the stacked (*S*) orientations. The small energy differences in the interchain interaction are introduced by the graphene substrate and can be attributed to inequivalent adsorption sites on graphene. These are likely to be modified in the case of incommensurate overlayers, which are known to form Moiré patterns in STM images.[8]

Considering a C_2H_4 unit of an isolated polyethylene chain, adsorption on graphene leads to an energy gain of 0.09 eV in the *S* orientation and 0.12 eV in the more stable *P* orientation. In view of the polyethylene-substrate attraction that is similar to the interchain attraction, we expect the formation of self-assembled monolayers forming both *S* and *P* domains on graphene. Due to their higher stability, *P* domains should prevail unless the system is subject to external constraints including lateral pressure.

Having established the optimum polymer arrangement within the polyethylene layers, we next address the preferential orientation of the polymer chains with respect to the graphene substrate. Different representative alignments for the two orientations are depicted in Fig. 3. The optimized adsorption geometry of polyethylene in the preferential parallel (*P*) orientation, lying down on graphene along the armchair direction, is depicted in Fig. 3(b), and the corresponding zigzag alignment is shown in Fig. 3(c). We should note that in the optimum adsorption geometry of *P*-oriented polyethylene (PE) aligned along the zigzag direction on graphene, the plane of the PE carbon backbone is tilted by 2.5° with respect to graphene, which will have important consequences for the STM images of alkane chains.

Energetically, we find zigzag aligned PE in Fig. 3(c) to be favored by 0.08 eV/C_2H_4 with respect to armchair aligned PE. The zigzag alignment represents the most favorable structure, since axial displacements of the chain reduce its binding energy by no more than 0.02 eV/C_2H_4, suggesting that even misaligned or displaced chains prefer the zigzag direction. As mentioned in the discussion of our results in Fig. 2, zigzag aligned polyethylene lying down parallel to graphene in Fig. 3(c) is energetically favored by 0.03 eV/C_2H_4 over polyethylene standing up normal to graphene in Fig. 3(d). Based on the hierarchy of interactions, we expect coexistence of polyethylene chains in *P* and *S* orientations, with zigzag and armchair alignment on the graphene substrate. The largest domains are expected for the stable *P*-oriented PE in zigzag alignment, the smallest domains for *S*-oriented PE in armchair alignment.

C. Bonding nature of long chain alkanes on graphite

The chemical origin of the adsorbate interaction with the graphene substrate is addressed in Fig. 4 for *P*-oriented polyethylene and in Fig. 5 for *S*-oriented polyethylene. The height of the polyethylene axis center above graphene is $h=3.4$ Å for *P*-oriented polyethylene and $h=3.8$ Å for *S*-oriented polyethylene. This relatively large adsorbate-substrate separation is consistent with the relatively small adsorption energy. The total charge densities in Figs. 4(c) and 5(c), and, in particular, the difference charge densities in Figs. 4(d) and 5(d) indicate that there is essentially no net charge transfer between adsorbate and substrate. Small, but nonzero values of the charge density difference in Figs. 4(d) and 5(d) are indicative of weak covalent bonds. The moderate charge density accumulation in the region between PE and graphene, observed in Fig. 4(d), explains the slightly

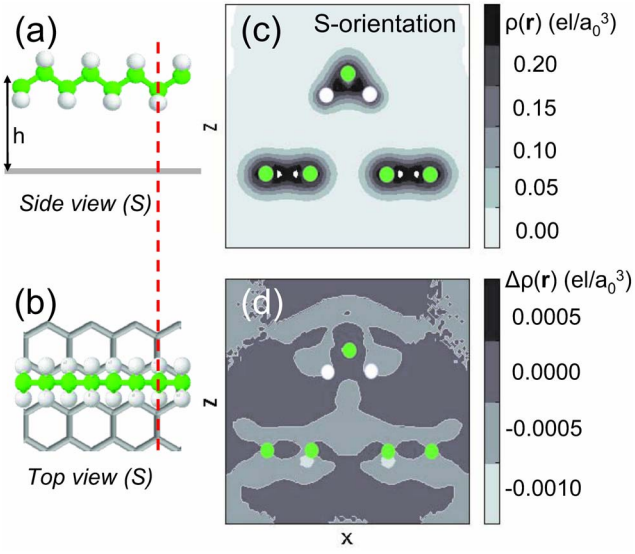

FIG. 5. (Color online) Nature of bonding of polyethylene in *S* orientation, standing normal to graphene. The polyethylene adsorption geometry on graphene, shown (a) in side view and (b) in top view. Contour plots of (c) the total charge density $\rho_{\mathrm{PE/gra}}(\mathbf{r})$ and (d) the charge density difference, defined as $\Delta\rho(\mathbf{r})=\rho_{\mathrm{PE/gra}}(\mathbf{r})-\rho_{\mathrm{PE}}(\mathbf{r})-\rho_{\mathrm{gra}}(\mathbf{r})$. The plane of the contour plots is normal to the polymer axis and is indicated by the dashed line in (a) and (b).

stronger adsorption bond in the *P* orientation. The weaker adsorption bond in the *S* orientation may be traced back to a moderate charge density depletion in the same region, observed in Fig. 5(d).

D. STM images of long chain alkane monolayers on graphite

To verify our results for the preferential adsorption geometry of polyethylene or finite alkane chains on graphene, we compare our optimized structures to STM images of the corresponding systems. Since scanning tunneling microscopy only images electronic states in the energy range $E_F - eV_{\mathrm{bias}} < E < E_F$, where V_{bias} is the bias voltage and E_F is the Fermi level, we must further inspect the electronic structure of polyethylene on graphene to interpret the images.

Results for the electronic density of states (DOS) of polyethylene on graphene are presented in Fig. 6. In Fig. 6(a), we compare the DOS of pristine graphene to polyethylene/graphene in *P* and *S* orientations. As seen in Fig. 1(b), polyethylene is a wide-gap insulator with a fundamental gap exceeding 7.5 eV and becomes visible to the STM only in the energy range, where the electronic states of PE-covered graphene display a significant PE character. We expect a nonvanishing polyethylene character at those energies, where the DOS of PE on graphene differs from the pristine graphene substrate. This can be best judged by inspecting the difference density of states ΔDOS for *P*-oriented PE in Fig. 6(b) and that of *S*-oriented PE in Fig. 6(c). These results suggest that no signal related to polyethylene should occur at bias voltages $V_{\mathrm{bias}} \lesssim 1.4$ V when imaging the occupied states.

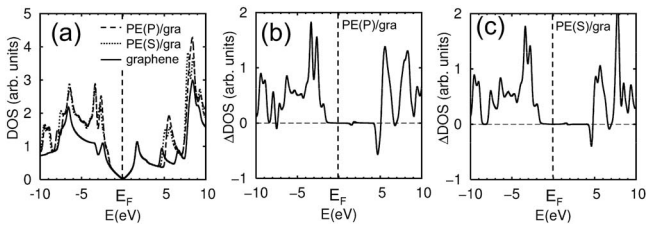

FIG. 6. (a) Density of states (DOS) of polyethylene (PE) monolayers in *P* and *S* orientation on graphene, compared to the DOS of pristine graphene. The DOS has been convoluted by 0.2 eV. (b) Difference density of states ΔDOS[PE(*P*)/gra]=DOS[PE(*P*)/gra]−DOS(graphene) for *P*-oriented PE. (c) Difference density of states ΔDOS[PE(*S*)/gra]=DOS[PE(*S*)/gra]−DOS(graphene) for *S*-oriented PE.

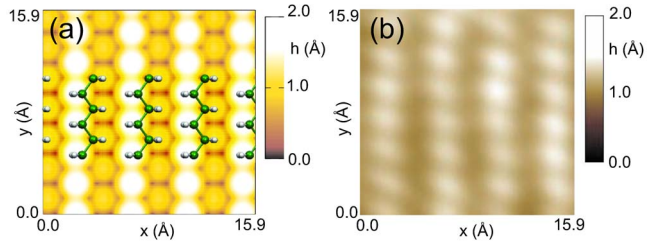

FIG. 7. (Color online) Scanning tunneling microscopy (STM) images of self-assembled alkane monolayers on graphene at the bias voltage $V_{\mathrm{bias}}=2.0$ V (sample negative). (a) Calculated STM image of a polyethylene (PE) monolayer on graphene, corresponding to a constant charge density $\rho_{\mathrm{STM}}=10^{-6}e/a_0^3$. The image is superimposed with the model of the PE structure. (b) STM image of a *n*-docosane monolayer on graphene, observed at the constant tunneling current of 215 pA.

Calculated and observed STM images of self-assembled alkane monolayers on graphene are shown in Fig. 7. STM images obtained in the constant current mode display changes of the tip height h as a function of the lateral tip position (x,y). The corresponding calculated images display the height $h(x,y)$ corresponding to a given value of the charge density ρ_{STM} that is associated with states in the range $E_F - eV_{\mathrm{bias}} < E < E_F$. The calculated STM image in Fig. 7(a), obtained for $V_{\mathrm{bias}}=2.0$ V and $\rho_{\mathrm{STM}}=10^{-6}e/a_0^3$, can be directly compared to STM images obtained in the constant-current mode at the same bias voltage. Superposed to the calculated image in Fig. 7(a) is the underlying structure of *P*-oriented polyethylene chains, aligned along the zigzag direction of graphene and separated by 4.26 Å, commensurate with the underlying graphene layer. Comparison between the calculated STM image and the underlying polymer structure indicates that the bright spots in the image closely correlate with the position of H atoms of the alkane chains. As mentioned above, due to the small horizontal tilt of polyethylene on graphene, the hydrogen atoms on the right-hand side of the polymer in Fig. 7(a) are closer to graphene by 0.2 Å and, thus, could naively be expected to be observed at a slightly smaller height than those on the left-hand side of the chains. At the finite bias voltage used in the STM, however, the height contours are not directly correlated with atomic positions. In the present case, the small height difference of 0.2 Å between the hydrogen atoms translates into a much larger apparent height difference of 0.6 Å in STM images observed at $V_{\mathrm{bias}}=2.0$ V.

Figure 7(b) shows STM data obtained when imaging a solution of *n*-docosane in 1-phenyloctane on graphite at $V_{\mathrm{bias}}=2.0$ V (sample negative), at the constant tunneling cur-

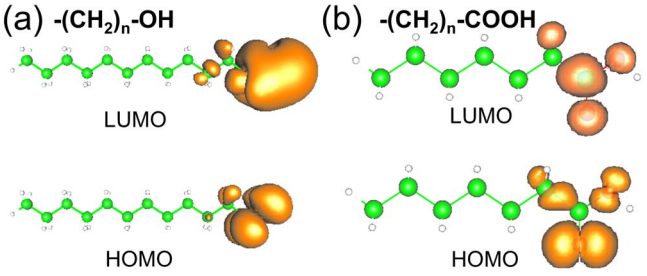

FIG. 8. (Color online) Highest occupied molecular orbital (HOMO) and lowest unoccupied molecular orbital (LUMO) of polyethylene chains terminated by (a) an OH group and (b) a COOH group. Charge density contours are superposed with ball-and-stick models of the molecules.

rent of 215 pA. The STM image, obtained using a tip submersed in the solution, shows a well-formed self-assembled monolayer of *n*-docosane, closely resembling the calculated image of Fig. 7(a) showing atomic resolution.

E. Structure and stability of long chain alkane derivatives on graphite

Next, we studied the effect of alcohol and carboxylic acid functional groups on the adsorption geometry and the corresponding STM images. Whereas the frontier orbitals of polyethylene or unmodified alkane chains extend along the entire chain, as seen in Figs. 1(c) and 1(d), this is generally not the case with molecules possessing terminal functional groups. Since frontier orbitals are very important for understanding the interaction and optimum alignment of molecules, we plot the charge density associated with the highest occupied molecular orbital (HOMO) and lowest unoccupied molecular orbital (LUMO) of polyethylene chains terminated by an OH group in Fig. 8(a) and those of COOH-terminated polyethylene in Fig. 8(b).

These functional groups introduce new localized states between the top of the valence and bottom of the conduction band of polyethylene, which become frontier states and reduce the fundamental gap. Inspection of Fig. 8 suggests that the frontier states are localized near the functional groups.

Possible adsorption arrangements of long chain alcohols within self-assembled monolayers on graphene are displayed in Fig. 9. The relative stability of the different arrangements depends on whether the alcohol functions are arranged head to head or head to tail within a domain, and also on the nature of the domain boundary. Relative stabilities of these systems are compared in Table I for the arrangements displayed in Fig. 9.

F. Domain formation in self-assembled monolayers of long chain alkane derivatives on graphite

Within an isolated domain, which contains head-to-head parallel or head-to-tail antiparallel OH-terminated alkanes, possible adsorption arrangements are displayed in Figs. 9(a)–9(c). The corresponding adsorption energy values in Table I suggest that the parallel arrangement of Fig. 9(a), with all alcohol ends aligning head to head along a domain edge normal to the chains, is the most stable. The staggered parallel arrangement of Fig. 9(b), with the domain edge at a

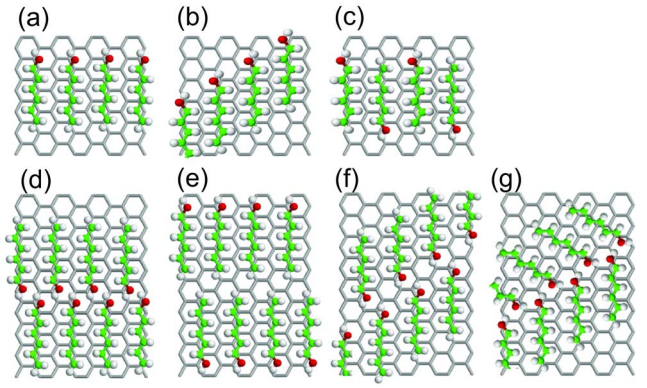

FIG. 9. (Color online) Adsorption arrangements in finite-width domains of straight chain alcohols in self-assembled monolayers on graphene. Common to all structures is the *P* orientation of the alkyl chains and their alignment along the zigzag direction on graphene. Adjacent chains within one domain can be parallel, with OH groups pointing in the same direction, or antiparallel, with OH groups pointing in the opposite directions.

30° angle to the chains, is the least stable. The antiparallel arrangement of Fig. 9(c), with the alcohol ends aligning head to tail along a domain edge normal to the chains, is not as stable as the parallel head-to-head arrangement of Fig. 9(a). Nevertheless, since it contains a shorter domain boundary than the staggered arrangement of Fig. 9(b), the arrangement of Fig. 9(c) lies energetically between those of Figs. 9(a) and 9(b).

Possible boundaries between domains of long chain alcohols are considered in Figs. 9(d)–9(g). All these arrangements are energetically preferred over those for a single domain with the energetically taxing open edge. In long chain alcohols, the OH bond direction forms a 60° angle to the axis of the alkyl chain. Among the many ways to assemble long chain alcohols into a monolayer superstructure, arrangements that form H bonds at the domain boundary are energetically preferred.[17] The chain directions within the SAMs are furthermore constrained by the symmetry of the underlying graphene lattice, which allows lamellar directions in adjacent domains to be either parallel or to form a 120° angle.

Figures 9(d) and 9(e) depict head-to-head and tail-to-tail alignment of long chain alcohols at the boundary of adjacent domains, in which all long chain alkyls are aligned parallel to one another. The head-to-head alignment provides additional hydrogen bonding at the interface, thus stabilizing the

TABLE I. Relative stability of finite-width domains of $C_6H_{13}OH$ in self-assembled monolayers on graphene. The structure labels correspond to the adsorption arrangements of Figs. 9(a)–9(g). The adsorption energy E_{ad} of $C_6H_{13}OH$ is given by $E_{ad}=E_{tot}(C_6H_{13}OH\ \text{array/graphene})-E_{tot}(\text{isolated } C_6H_{13}OH \text{ in vacuum})-E_{tot}(\text{graphene})$.

Structure	E_{ad} (eV)
(a)	−1.00
(b)	−0.95
(c)	−0.98
(d)	−1.45
(e)	−1.03
(f)	−1.20
(g)	−1.60

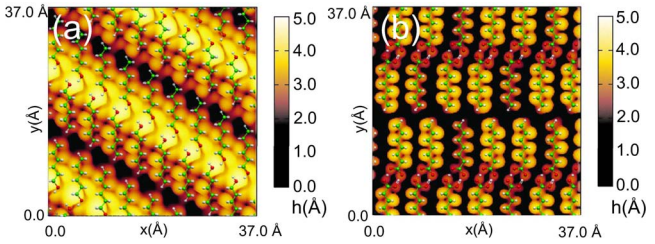

FIG. 10. (Color online) Calculated STM images of alkane derivatives forming self-assembled monolayers on graphene. (a) $C_6H_{13}OH$ at the bias voltage $V_{bias}=1.6$ V; (b) $C_6H_{13}COOH$ at $V_{bias}=1.3$ V (sample negative). Charge density contours for $\rho_{STM}=10^{-6}e/a_0^3$ are superimposed with structural models. The y axis is aligned along the zigzag direction of the underlying graphene.

structure of Fig. 9(d) over that of Fig. 9(c). In the arrangement of Fig. 9(f), the parallel alignment of all long chain alcohols in adjacent domains is maintained, but the domain boundary is rotated by 30° with respect to the alkyl axis. Even though hydrogen bonding stabilizes this arrangement over that of Fig. 9(e), the longer boundary length makes it energetically unfavorable relative to the arrangement of Fig. 9(d).

The symmetry of the underlying graphene lattice also allows long chain alcohols of two different domains to meet at a 120° angle, as shown in Fig. 9(g). Since the arrangement of the terminal OH groups at the domain boundary in Fig. 9(g) is most favorable among all the arrangements discussed here, we expect it to occur frequently in the self-assembled monolayers.

Our findings for self-assembled monolayers of alkane derivatives with COOH functional groups are qualitatively similar to those discussed in Fig. 9. However, the energy to separate a pair of facing carboxylic acid molecules (so-called carboxylic acid dimers), $\Delta E_b=-1.72$ eV, is more than three times larger than the separation energy $\Delta E_b=-0.47$ eV of a pair of facing alcohol molecules.

G. STM images of monolayers of long chain alkane derivatives on graphite

To help identify the location of OH and COOH functional groups in self-assembled monolayers of long chain alcohols and carboxylic acids, we calculated the corresponding STM images of $C_6H_{13}OH$ and $C_6H_{13}COOH$ assemblies on graphene. Our results, shown in Fig. 10, suggest that the OH terminal group should appear at a larger apparent height, whereas the COOH group should appear at a smaller apparent height than the alkane chain in STM images obtained in the constant current mode.

Figure 11 displays STM images and the corresponding structural models of self-assembled monolayers of 1-docosanol ($C_{22}H_{45}OH$) and 1-docosanoic acid ($C_{22}H_{45}COOH$) molecules on graphite. According to Fig. 7, we associate the lamellar structure with parallel alkane chains. For illustration purposes, the length of fully stretched (all *s-trans* conformations) docosanol ($l=29.5$ Å) and docosanoic acid ($l=30.8$ Å) molecules is indicated in the figure. The STM images in Figs. 11(a) and 11(c) suggest the presence of stripe-shaped domains that are split in the middle

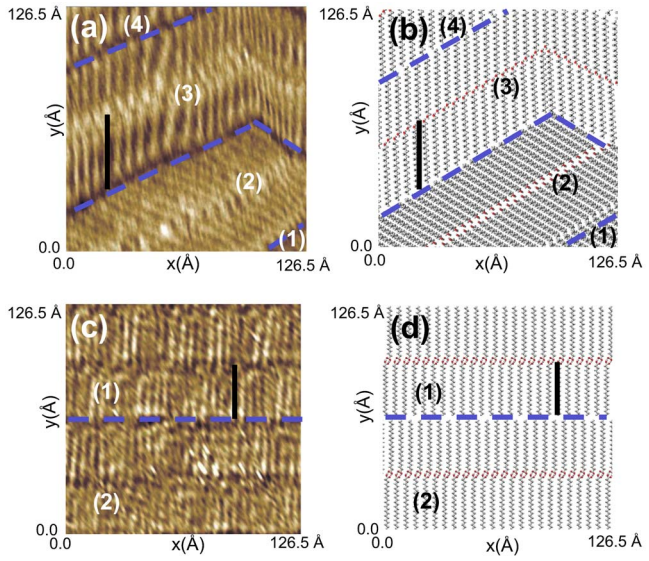

FIG. 11. (Color online) STM images [(a) and (c)] and structural models [(b) and (d)] of alkane derivatives forming self-assembled monolayers (SAMs) on graphite. (a) Observed and (b) model structure of 1-docosanol ($C_{22}H_{45}OH$) on graphite. (c) Observed and (d) model structure of 1-docosanoic acid ($C_{22}H_{45}COOH$) on graphite. The STM image (a) was obtained using the bias voltage 1.6 V (sample negative) at the constant tunneling current of 30 pA, the STM image (c) was obtained using 1.3 V (sample negative) bias and a 25 pA current. Domains are labeled by numbers. The size of individual molecules is indicated by a black rectangle in each panel. The OH and COOH terminal groups are emphasized in red in (b) and (d), and the domain boundaries are indicated by the heavy dashed lines.

into subdomains spanned by parallel arrays of the alkane derivatives.

According to our calculations, the equilibrium separation between docosanol chains in the *S* orientation is 3.50 Å, incommensurate with the graphene lattice, which agrees well with the interchain separation in domains (1) and (2) of Fig. 11(a). Similarly, our predicted equilibrium separation of *P*-oriented docosanol chains of 4.26 Å agrees well with the observed interchain separation in domains (3) and (4) of Fig. 11(a). Our energy results in Table I suggest that hydrogen bonds stabilize the interface between adjacent domains of head-to-head aligned long chain alcohols. As a plausible working hypothesis, we will assume that the subdomains in Fig. 11(a) contain OH groups at both sides of the interface, with hydrogen bonds acting as a stabilizing element of the semirigid domain backbone. This assumption is confirmed by the observation of the largest apparent height in the STM image of Fig. 11(a) in the middle of the domains, in accordance with the predicted STM images for this molecular arrangement, shown in Fig. 10(a). Combining all this information is sufficient to present a well-defined structural counterpart to the STM image of Figs. 11(a) in Fig. 11(b).

A similar interpretation can be applied to the STM image of docosanoic acid monolayers in Fig. 11(c). The predicted equilibrium separation between *P*-oriented docosanoic acid chains in the *P* orientation is 5.50 Å, incommensurate with the graphene lattice, which agrees well with the interchain separation in the domains of Fig. 11(c). Also, in this case, the domains are stripe shaped and contain two subdomains, each spanned by an array of docosanoic acid molecules. As in the

case of the alcohol terminal group, the acid groups favor a head-to-head configuration at the interface of the subdomains, which provides the domain with a stabilizing backbone. Unlike in alcohols, where the chains may either be parallel or form a 120° angle, the alkyl chains in carboxylic acid SAMs have a strong energetic preference for being parallel. Also, the interaction between head-to-head acid terminal groups of alkanes is more than three times larger than in the alcohols, resulting in a very rigid, straight domain backbone that is normal to the chain direction. The postulated head-to-head alignment of the acid groups in the middle of the domain cannot be verified easily, since the predicted apparent height of the acid terminal group in STM images of monolayers is only slightly smaller than that of the alkane, showing very little contrast.

V. DISCUSSION

The favored structure of bulk polymer melts at high temperatures is known to depend largely on entropy. We believe that the relevant degrees of freedom are largely frozen out when polymers self-assemble to ordered monolayers on a substrate, thus significantly reducing the configurational part of entropy. We furthermore assume that other contributions, including configurational entropy, may be nearly equal in systems we compare, thus justifying *a posteriori* our discussion of stability differences based on total energy calculations performed at $T=0$.

The formation of ordered overlayers of long chain alkanes and their derivatives on graphite out of their solution in phenyloctane is a slow process. After an initial fast adsorption stage, it takes several minutes at room temperature to complete the ordering in the self-assembled monolayers. Once a domain structure is formed, domain walls are observed to move in time.[8] Assuming that the presence of the solvent does not affect the adsorption energy hierarchy in Table I, the most stable structure at $T=0$ would consist of infinite stripe domains. The favored lamellar structure of long chain alcohols would be a 120° chevron pattern, locally represented in Fig. 9(g). In the corresponding structure of long chain acids, the lamellae should be all parallel and aligned normal to the domain walls, as seen in Fig. 9(d). At nonzero temperatures, configurational entropy should introduce roughening of the domain walls. Moreover, the assumption that the solvent does not affect the adsorption geometry hierarchy is not very well founded, since the adsorption energy of phenyloctane molecules on graphite is only slightly smaller than that of alkanes and their derivatives of a comparable size. Thus, the real SAM patterns may deviate on energy and entropy grounds from the $T=0$ equilibrium structure.

In reality, the origin of the complex patterns in Figs. 11(a) and 11(b) is only partly related to stability issues, since the relatively slow self-assembly process has an important kinetic component. Alkane chains are likely to adsorb simultaneously at different substrate locations and assemble to domains that grow in size, until they hit the next domain. At this moment, the two domains will attempt to minimize the interface energy by local rearrangements. Since the assembly process is relatively slow, we expect these rearrangements not to yield the globally optimized structure. In general, we expect an energy-related compromise structure of the adsorbate layer subdivided into large domains with straight edges. Energetic compromises, resulting in a complete monolayer coverage, may include unfavorable adsorbate orientation, including the *S*-oriented domains (1) and (2) in Figs. 11(a) and 11(b) that may form under lateral pressure. Rather than forming void islands, the system may accept the formation of energetically unfavorable domain wall boundaries, such as that between domains (2) and (3) in Figs. 11(a) and 11(b).

As mentioned above, the strong interaction between head-to-head terminal groups of long chain acids favors only one domain structure with all chains parallel and the domain boundaries normal to the chain direction. Due to the high stability and rigidity of this assembly, we expect straight stripe domains to cover the entire sample, with diminished effects of entropy, presence of the solvent, or kinetics. Indeed, the pattern observed in Fig. 11(c) is nearly free from defects and is identical to the optimum structure expected at $T=0$.

VI. SUMMARY AND CONCLUSIONS

In summary, we combined scanning tunneling microscopy observations with *ab initio* calculations to study the self-assembly of long chain alkanes and their derivatives on graphite. We identified the optimum adsorption geometry of polyethylene, long chain alkanes, alcohols, and carboxylic acids on graphite. Calculated adsorption energies in different arrangements were used to predict the optimum structure of self-assembled monolayers. Theoretical predictions for STM images of optimized adsorbate overlayers were compared to the experimental data for docosane, docosanol, and docosanoic acid on graphite. Our total energy results provided a sound base for interpreting the observed domain wall structure in the self-assembled monolayers. In particular, we found that the observed domain wall structure in docosanol SAM superstructures should vary from sample to sample, since kinetic processes are as important as structural stability. In docosanoic acid SAM superstructures, the interaction between COOH terminal groups at the domain wall boundary is much stronger, resulting in patterns reflecting the globally optimized structure, with no sample-to-sample domain variation. These results can be directly used when designing templates to be used in template directed nanoassembly and transfer processes. Finally, since nearly any nanoparticle can be attached to long chain molecules, including those described here, self-assembly of such molecules or polymers provides an efficient means to prepare ordered arrays of uniformly spaced nanoparticles.

ACKNOWLEDGMENTS

We thank Kiseok Chang for assistance with the graphical representation of STM images. G.M., D.T., and S.B., acknowledge financial support from the Nanoscale Science and Engineering Center for High-rate Nanomanufacturing (NSF NSEC Grant No. 425826). T.Y., D.T., and S.B., also ac-

knowledge additional support from the National Science Foundation (NSF-NIRT Grant No. ECS-0506309).

[1] P. Ball, *The Self-Made Tapestry: Pattern Formation in Nature* (Oxford University Press, Oxford, 2001).
[2] A. E. Busnaina, *Nanomanufacturing Handbook* (CRC, Boca Raton, FL, 2006).
[3] R. D. Piner, J. Zhu, F. Xu, S. Hong, and C. A. Mirkin, Science **283**, 661 (1999).
[4] J.-F. Liu and G. P. Miller, J. Phys. Chem. C **111**, 10758 (2007).
[5] J. S. Foster and J. E. Frommer, Nature (London) **333**, 542 (1988).
[6] T. Muller, T. L. Werblowsky, G. M. Florio, B. J. Berne, and G. W. Flynn, Proc. Natl. Acad. Sci. U.S.A. **102**, 5315 (2005).
[7] D. M. Cyr, B. Venkataraman, and G. W. Flynn, Chem. Mater. **8**, 1600 (1996).
[8] J. P. Rabe and S. Buchholz, Science **253**, 424 (1991).
[9] Density functional theory (DFT) is best known for its structural predictions in covalently bonded systems. Within the local density approximation (LDA), DFT is moreover known to correctly reproduce even the equilibrium structure of weakly interacting systems such as graphite that are held together—to an important degree—by van der Waals forces. In reality, van der Waals forces are not neglected in DFT but enter in an approximate way through the exchange-correlation functional.
[10] J. P. Perdew and A. Zunger, Phys. Rev. B **23**, 5048 (1981).
[11] J. M. Soler, E. Artacho, J. D. Gale, A. García, J. Junquera, P. Ordejón, and D. Sánchez-Portal, J. Phys.: Condens. Matter **14**, 2745 (2002).
[12] S. F. Boys and F. Bernardi, Mol. Phys. **19**, 553 (1970).
[13] N. Troullier and J. L. Martins, Phys. Rev. B **43**, 1993 (1991).
[14] L. Kleinman and D. M. Bylander, Phys. Rev. Lett. **48**, 1425 (1982).
[15] G. C. McGonigal, R. H. Bernhardt, and D. J. Thomson, Appl. Phys. Lett. **57**, 28 (1990).
[16] W. Liang, M. H. Whangbo, A. Wawkuschewski, H. J. Cantow, and S. N. Magonov, Adv. Mater. (Weinheim, Ger.) **5**, 817 (1993).
[17] S. Abrahamsson, G. Larsson, and E. Vonsydow, Acta Crystallogr. **13**, 770 (1960).